KSCE Journal of Civil Engineering 29 (2025) 100132

Contents lists available at ScienceDirect

KSCE Journal of Civil Engineering

journal homepage: www.elsevier.com/locate/kscej

Generic predictive model for shear wave velocity profile at shallow depths in South Korea

Jieun Kim, Byungmin Kim, Youngkyu Cho *

Department of Civil Urban Earth and Environmental Engineering, Ulsan National Institute of Science and Technology, Ulsan, South Korea 44919

ARTICLE INFO

Keywords:
Shear wave velocity profiles in South Korea
Predictive model
Shallow bedrock depth
Regression analysis

ABSTRACT

It is essential to adequately characterize the surface ground motion at sites for earthquake-resistant analysis and infrastructure design. The incorporation of the spatial variability of shear wave velocity (V_S) profiles within a given site into the seismic site response analysis has become increasingly crucial. This study proposes a V_S profile prediction model suitable for Korean regions conditioned on the time-averaged V_S over the top 30 m (V_{S30}). We collected 702 V_S profiles across South Korea and fitted them to the analytical function proposed by a previous study, the parameters of which are subsequently regressed on V_{S30}. The V_S profiles predicted using the model with the derived parameters are remarkably similar to the measured V_S profiles not included in curve fitting. The goodness-of-fit scores for the proposed model's predictions relative to the measured V_S profiles exhibit an improvement of approximately 6 and 10 % compared to the V_S profiles predicted by the model of a previous study. This model is expected to be used for preliminary assessments of site amplification alongside methods for predicting V_{S30} or the previously evaluated experimental dispersion curves or V_S profiles available from a site adjacent to the target sites.

1. Introduction

Moderate-size earthquakes occurred in Gyeongju in 2016 and Pohang in 2017, with local magnitudes of 5.8 and 5.4 in South Korea, respectively, which are uncommon in low seismicity regions. Societal awareness of seismic hazards and risks has increased substantially since these events, demanding enhancements in infrastructure safety against earthquakes. The fundamental objective of seismic analysis and design for the infrastructures is to predict surface ground shaking at sites of interest (or site amplification), commonly assessed through one-dimensional site response analysis (SRA). An indispensable input parameter for SRA is the shear wave velocity (V_S) profile, which is generally evaluated from field tests [e.g., downhole (DH), crosshole, suspension PS logging tests (invasive methods) and spectral/multi-channel analysis of surface wave (SASW/MASW) tests, and microtremor array measurement (MAM) (non-invasive methods)].

The V_S profile is spatially variable within a particular site, subsequently introducing uncertainty into site amplification (Pehlivan et al., 2015; Rathje et al., 2010). Accordingly, the incorporation of this variability into SRA has become crucial for more reliable estimations of site amplification, particularly at locations with sparse historical ground motion records. For instance, the necessity of this incorporation has been demonstrated through site-specific SRA integrated into probabilistic seismic hazard analysis (Rathje et al., 2015; Ansal et al., 2018), which involved multiple V_S measurements at a site of interest. However, addressing this variability using multiple field tests within a given site is challenging (i.e., performing more than 20 tests is considered inefficient and uneconomical).

Toro (1995) introduced a randomization model for the V_S profile in California. Shi and Asimaki (2018) proposed a generic prediction model for V_S profiles with more V_S profiles compiled in the California regions (for its V_S profile model, herein after referred to as the SA 18 model). Passeri et al. (2020) developed a predictive model for V_S profiles in Italy to consider the spatial variability. Marafi et al. (2021) developed a V_S profile prediction model for the Cascadia region of North America, inspired by the approach used in the SA 18 model. They incorporate both the time-averaged V_S over a 30 m depth (V_{S30}) and a deeper geological structure, represented by the depth at which V_S reaches 1.0 km/s ($Z_{1.0}$). These models were derived to offer a viable supplement to reduce the extensive measurements of V_S profiles (i.e., situations wherein conducting more than 20 invasive or non-invasive tests is unavailable) to predict the surface ground motions or assess regional-scale

* Corresponding author.
E-mail address: youngkyu@unist.ac.kr (Y. Cho).

https://doi.org/10.1016/j.kscej.2024.100132
Received 22 April 2024; Received in revised form 19 August 2024; Accepted 5 November 2024
Available online 27 November 2024

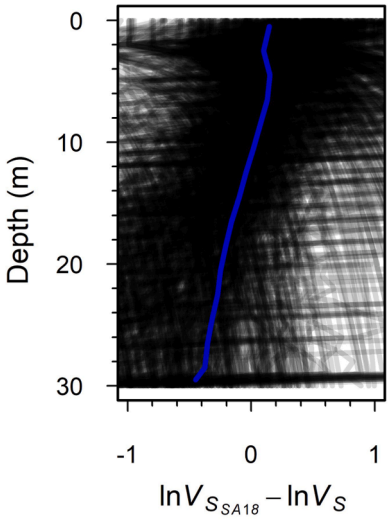

Fig. 1. Residuals of V_S profiles predicted by SA 18 model for 702 V_S profiles collected in South Korea (The individual residuals and its mean are represented by transparent gray and blue solid lines, respectively).

seismic hazards.

Kim and Yoon (2006) and Ahn et al. (2021) indicated that $V_S \geq 760$ m/s [commonly regarded as the engineering bedrock, FEMA (2020)] is mostly encountered at depths shallower than a 30 m in South Korea. Because the SA 18 model, a function of V_{S30}, was derived from a database of V_S profiles for sedimentary basins in California, its direct application to sites in South Korea may be inappropriate due to engineering bedrock at shallow depths. To illustrate this, we evaluated the residuals of the 702 V_S profiles compiled for this study against the SA 18 model using a natural logarithmic scale, as shown in Fig. 1. The mean residual (blue solid line) is slightly overestimated in the range of 0–13 m (a mean of +0.16), but it gradually decreases as the depth increases, reaching the smallest value (–0.36) at a depth of 30 m. Given the characteristics of V_S profiles in South Korea with the presence of bedrock at shallow depths, this implies that the V_S profiles in South Korea can be overpredicted and underpredicted by approximately 16.0 and 19.0 % on average within 0–13 m and 13–30 m, respectively, when using the SA 18 model.

This study derives the model parameters of the SA 18 model that are compatible with the V_S profiles in South Korea, enabling appropriate applications at Korean sites. This type of predictive model has never been proposed for V_S profiles at Korean sites. SA 18 model is selected since a single independent variable (V_{S30}) in its functional form is considered efficient for estimating the V_S profile in engineering applications, such as a preliminary design assessment or forward analysis. We collected 702 V_S profiles evenly distributed across South Korea. All the obtained V_S profiles were categorized based on the presence of $V_S \geq 760$ m/s at depths deeper or shallower than a depth of 30 m by denoting the depth with $V_S \geq 760$ m/s as Z_{760} (i.e., $Z_{760} > 30$ m and $Z_{760} \leq 30$ m, respectively). The V_S profiles within the two categories were then grouped by their V_{S30} values. The averaged V_S profiles within the V_{S30} groups were calculated and fitted to the SA 18 model. The derived model parameters were regressed against the V_{S30} values of the averaged V_S profile within each group. The V_S profiles predicted by the SA 18 model using the derived parameters, were validated against the averaged V_S profiles using a measure of goodness of fit.

2. Database of V_S profiles in South Korea

Numerous V_S profiles from various regions in South Korea have been accumulated over the past few decades. Three datasets of V_S profile measurements were obtained from 1) the Ministry of Interior and Safety (https://www.data.go.kr/index.do, 484 profiles by DH test; 2) the Ministry of Land, Infrastructure, and Transport (https://www.geoinfo.or.kr, 207 profiles by DH test); and 3) this research team (232 profiles performed by SASW and MASW). In total, 923 profiles were compiled. The variability in the V_S profiles by the DH and surface wave tests is known to be comparable, although the DH test yields less accurate estimates at depths of 2–4 m owing to the unknown propagation of stress waves between the surface source and the receiver in the borehole

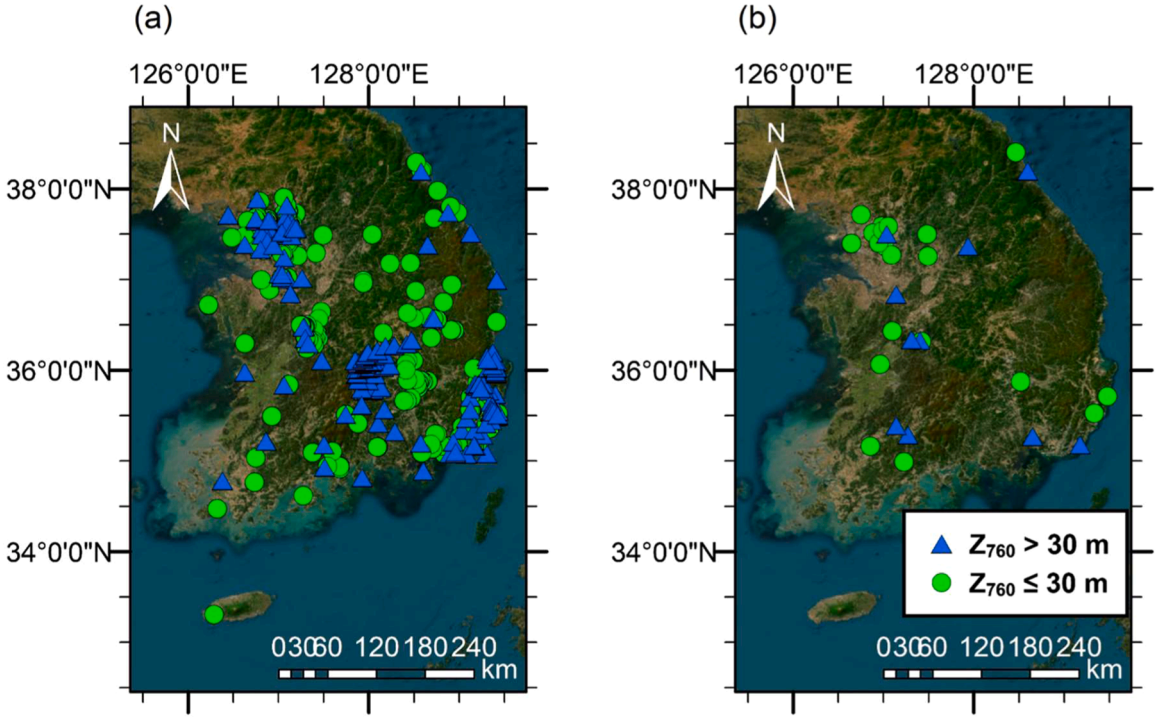

Fig. 2. Map showing locations of the collected 702 V_S profiles.

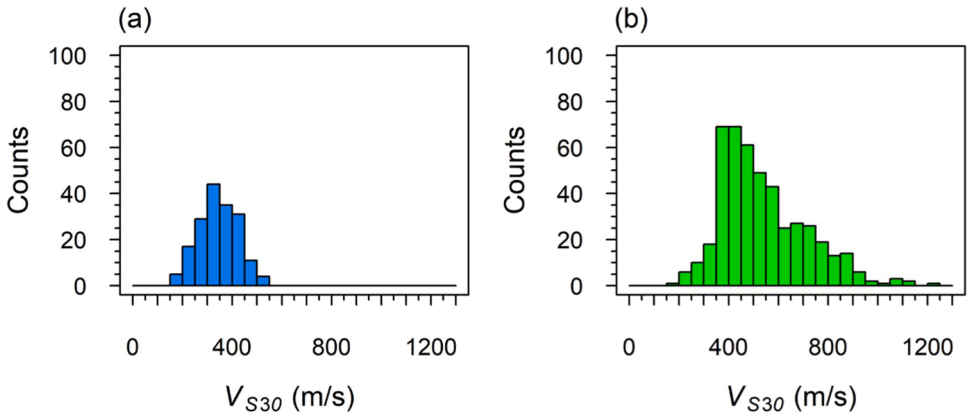

Fig. 3. Histograms of V_{S30} for the collected 702 V_S profiles: (a) $Z_{760} > 30$ m and (b) $Z_{760} \leq 30$ m.

Table 1
Minimum and maximum V_{S30}, V_{S30} of the averaged V_S profile, logarithmic standard deviation of V_S averaged over the depths ($\sigma_{\ln V_S}$), and goodness-of-fit measure ($\boldsymbol{gof}_{V_S}$) within each V_{S30} group for $Z_{760} > 30$ m.

No.	Minimum V_{S30} (m/s)	Maximum V_{S30} (m/s)	Averaged profiles' V_{S30} (m/s)	$\sigma_{\ln V_S}$
1	161.7	215.9	207.6	0.19
2	161.7	242.8	223.5	0.22
3	255.7	299.0	299.9	0.25
4	300.8	347.7	345.1	0.19
5	351.8	399.0	400.5	0.17
6	402.2	447.3	451.7	0.15
7	450.5	596.6	490.6	0.13
8	480.8	596.6	522.2	0.10

Table 2
Minimum and maximum V_{S30}, V_{S30} of the averaged V_S profile and logarithmic standard deviation of V_S averaged over the depths ($\sigma_{\ln V_S}$) within each V_{S30} group for $Z_{760} \leq 30$ m.

No.	Minimum V_{S30} (m/s)	Maximum V_{S30} (m/s)	Averaged profiles' V_{S30} (m/s)	$\sigma_{\ln V_S}$
1	179.0	369.5	353.3	0.33
2	360.5	399.8	414.3	0.25
3	400.5	499.8	499.5	0.30
4	500.8	599.6	602.4	0.29
5	550.8	646.5	670.5	0.30
6	600.6	646.5	707.1	0.30
7	600.6	697.5	758.5	0.32
8	701.5	796.4	846.1	0.27
9	725.3	804.2	862.0	0.28
10	760.2	858.8	905.1	0.27
11	803.1	891.7	937.4	0.22
12	853.0	946.0	977.3	0.19
13	862.9	999.0	1,018.8	0.19
14	923.4	1,226.1	1,133.0	0.24
15	996.1	1,226.1	1,232.1	0.24

(Garofalo et al., 2016). Hence, the V_S profiles from both methods can be integrated to derive the model parameters without differentiating between them. The compiled V_S profiles were mostly evaluated up to approximately 30 m depths, whereas a few V_S profiles extended to greater depths, ranging as 50–100 m. However, we used the V_S profiles up to depths of 30 m for model development to avoid any bias in the fitting (underestimation or overestimation) beyond this depth. In addition, a small number of profiles with $V_S < 100$ m/s at the top were excluded to achieve an unbiased estimate at the ground surface. Consequently, 702 V_S profiles were selected to estimate the parameters of the SA 18 model. Fig. 2 shows the locations of the 702 V_S profiles uniformly distributed across South Korea.

Here, 32.5 % of the V_S profiles (228) indicate that Z_{760} are greater than a depth of 30 m. However, most (67.5 %, 474) reveal that Z_{760} are present at points shallower than a depth of 30 m. Notably, a comparably large portion of V_S profiles with $Z_{760} \leq 30$ m corresponds to the observations by Kim and Yoon (2006) and Ahn et al. (2021). Hence, the V_S profiles were classified based on Z_{760} (i.e., $Z_{760} > 30$ m and $Z_{760} \leq 30$ m). Fig. 3 shows the histograms of V_{S30} of the V_S profiles for $Z_{760} > 30$ m and $Z_{760} \leq 30$ m. For $Z_{760} > 30$ m, V_{S30} follows a normal distribution, ranging as 162–597 m/s with a mean of 346 m/s and the 1st and 3rd quartiles (Q1 and Q3) of 285 and 411 m/s, respectively. For $Z_{760} \leq 30$ m, V_{S30} varies as 179–1,226 m/s with a mean of 547 m/s and Q1 and Q3 of 414 and 661 m/s, respectively, exhibiting a rough normal distribution.

3. Derivation of parameters for SA 18 model

The SA 18 model was derived from the analytical relationship between elastic wave velocity and depth proposed by Vrettos (1996) to predict a one-dimensional V_S profile for a sedimentary basin in the California region as follows:

$$V_S(z) = \begin{cases} V_{S0}\ , \ 0 \leq z \leq 2.5\ m \\ V_{S0}(1 + k(z - 2.5))^{\frac{1}{n}}\ , \ z > 2.5\ m \end{cases} \quad (1)$$

where z is the depth (m), V_{S0} is the assumed constant average V_S within 0–2.5 m, k dominates the rate of change of V_S (hereafter, the V_S slope) near the surface, and n determines the degree of curvature (i.e., the variation in the V_S slope at great depths). The curve shapes for $n > 1$, $n = 1$, and $n < 1$ correspond to concave downward (i.e., the V_S slope decreases with depth), straight line (the V_S slope is constant with depth), and concave upward (i.e., the V_S slope increases with depth), respectively. These three model parameters (V_{S0}, k, and n) are correlated with V_{S30}. Assuming that V_S is log-normally distributed, as described by Toro (1995), we calculated the averaged V_S (AVG_{V_S}) along the depths within each V_{S30} group as follows:

$$AVG_{V_S} = exp\left(\mu_{\ln(V_S)} + \frac{\sigma^2_{\ln(V_S)}}{2}\right) \quad (2)$$

where $\mu_{\ln(V_S)}$ and $\sigma_{\ln(V_S)}$ are the mean and standard deviation of $\ln(V_S)$ (normal distribution), respectively.

To derive the model parameters compatible with the V_S profiles in South Korea, the collected V_S profiles were grouped into a set of V_{S30} groups. Therefore, V_{S30} was calculated for each V_S profile. The range of V_{S30} (maximum V_{S30} – minimum V_{S30}) was divided into n bins (V_{S30} bins). We examined the relationship between V_{S0}, k, n and V_{S30} derived from fitting the averaged V_S profiles in each V_{S30} group (i.e., the initial V_{S30} bins) to Eq. (1). We adjusted the boundary values for each V_{S30} bin,

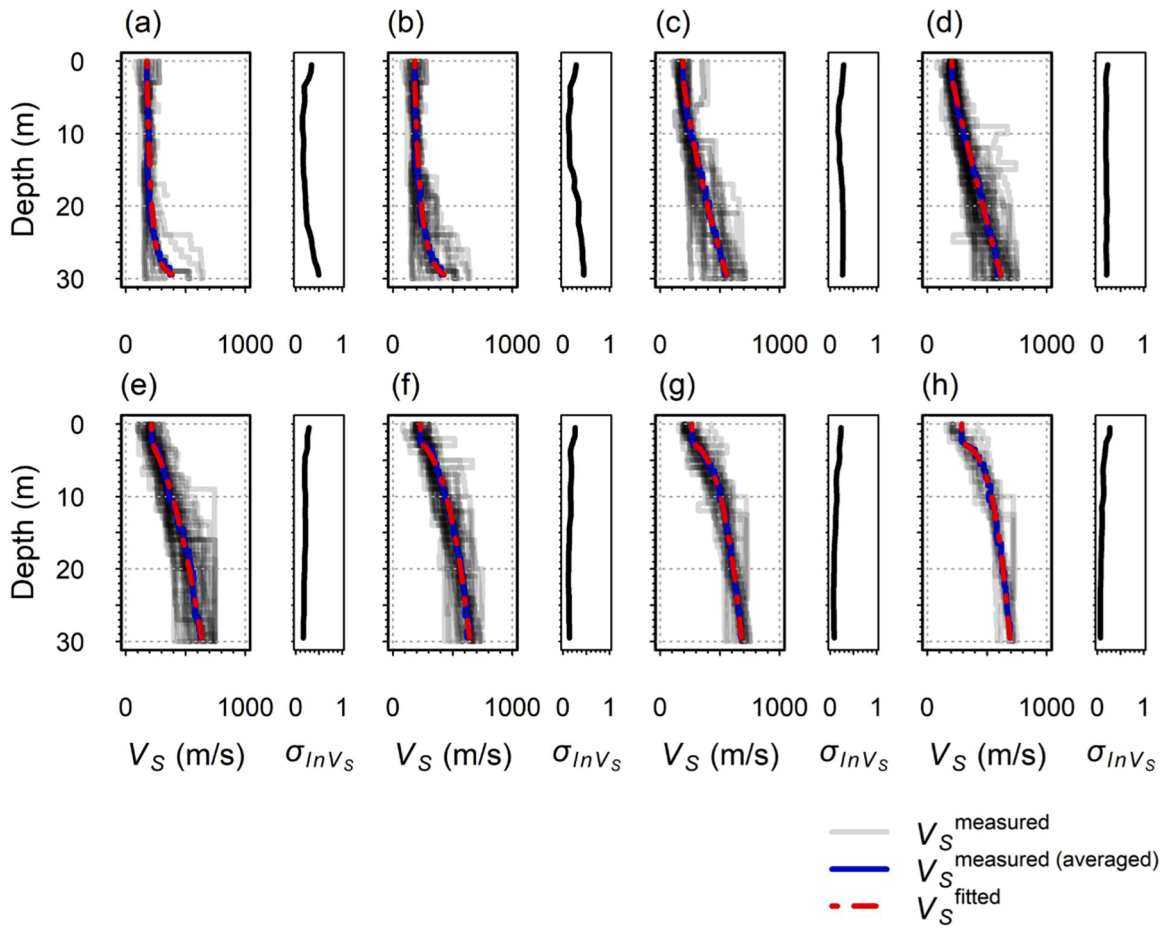

Fig. 4. Individual V_S profiles (transparent gray, solid lines) for each V_{S30} group of $Z_{760} > 30$ m alongside the averaged V_S profiles (blue, solid line) and the fitted V_S profiles (red, dash-dotted line). Constant, average values were computed within 0–2.5 m. The logarithmic standard deviation of individual V_S profiles ($\sigma_{\ln V_S}$) with depth is shown by black solid line on the right of each V_S profile panel.

allowing for a few V_S profiles to overlap in the V_{S30} bin's boundaries (i.e., included more than once in adjacent V_{S30} bins). We iterated the curve fitting process and the examination of the relationship between V_{S0}, k, n and V_{S30} until the optimal correlation was achieved (i.e., iterating the binning process). Each V_{S30} group contains at least 10 V_S profiles to ensure a statistically unbiased/robust estimation. Through the trial and error in V_{S30} binning process, we consequently attained the eight and fifteen groups for $Z_{760} > 30$ m and $Z_{760} \leq 30$ m, respectively. Tables 1 and 2 list the minimum and maximum V_{S30}, V_{S30} of the averaged V_S profile, and the mean logarithmic standard deviation of V_S over the depths for each group for $Z_{760} > 30$ m and $Z_{760} \leq 30$ m, respectively.

Figs. 4 and 5 show the individual V_S profiles (transparent gray, solid lines) along with the averaged V_S profile (blue, solid line), the V_S profile fitted using Eq. (1) (red, dash-dotted line), and the $\sigma_{\ln V_S}$ profile within each V_{S30} group for $Z_{760} > 30$ m and $Z_{760} \leq 30$ m, respectively. For $Z_{760} > 30$ m, the averaged V_S profiles of groups 1 and 2 remain approximately constant within 2.5–20 m, with the variation in the V_S slope slightly increasing below 20 m (Fig. 4a and b). The groups 3 and 4 (Fig. 4c and d) exhibit an approximately linear increase in the averaged V_S profiles within 2.5–30 m. The remaining V_{S30} groups (Fig. 4e–h) exhibit averaged V_S profiles with the relatively large V_S slope at shallow depths whereas the variation in the V_S slope diminishes as depth approaches 30 m. For $Z_{760} \leq 30$ m, the averaged V_S profile of the first and second groups (Fig. 5a and b) do not vary appreciably within 2.5–13 m, followed by an increase in the variation in the V_S slope beyond 13 m. The averaged V_S profiles of groups 3–6 (Fig. 5c–f) exhibit a gentle V_S slope at shallow depths, whereas the variation in the V_S slope with depth transitions from approximately constant to decreasing as V_{S30} increases. Fig. 5g–o show that the V_S slope at shallow depths for the averaged V_S profiles increases with V_{S30} and that the variation in the V_S slope with depth decreases with V_{S30}. The $\sigma_{\ln V_S}$ profiles typically decrease or are approximately constant with the depth aside from a few groups (Figs. 4a and b and 5a and b). We computed the mean $\sigma_{\ln V_S}$ over the depths for each V_{S30} group, with the resulting values listed in Tables 1 and 2 for $Z_{760} > 30$ m and $Z_{760} \leq 30$ m, respectively. These mean $\sigma_{\ln V_S}$ values range as 0.1–0.25 for $Z_{760} > 30$ m and as 0.19–0.33 for $Z_{760} \leq 30$ m.

V_{S0}, k, and n were estimated by fitting the averaged V_S profile within each group using Eq. (1). Their correlations with the V_{S30} of the averaged V_S profiles are illustrated in Figs. 6 and 7 for $Z_{760} > 30$ m and $Z_{760} \leq 30$ m, respectively. The trends observed in the averaged V_S profiles across groups in Figs. 4 and 5 are manifested in the resulting values of V_{S0}, k, and n. V_{S0} increases with increasing V_{S30}, suggesting that the average V_S near the surface tends to increase with increase in the mean stiffness of site for both $Z_{760} > 30$ m and $Z_{760} \leq 30$ m. Increasing k with V_{S30} implies a rapid variation in the V_S at shallow depths (i.e., V_S slope becoming large) as the mean stiffness of site increases. A minimal change in the V_S at shallow depths for soil sites ($V_{S30} < 760$ m/s) of both $Z_{760} > 30$ m and $Z_{760} \leq 30$ m (k for both ranges analogously as 0–5) compared to a more rapid variation in V_S at shallow depths (k range of 5–60) for rock sites ($Z_{760} \leq 30$ m with $V_{S30} \geq 760$ m/s). The values of n are below unity (concave upward) when V_{S30} is smaller than approximately 400 and 500 m/s for $Z_{760} > 30$ m and $Z_{760} \leq 30$ m, respectively, whereas the n values are greater than one (concave downward) beyond those two V_{S30} values for each Z_{760} category. We derived the analytical functions that can capture the relationships between the three parameters (V_{S0}, k, n) and the averaged profiles' V_{S30} of each group using the

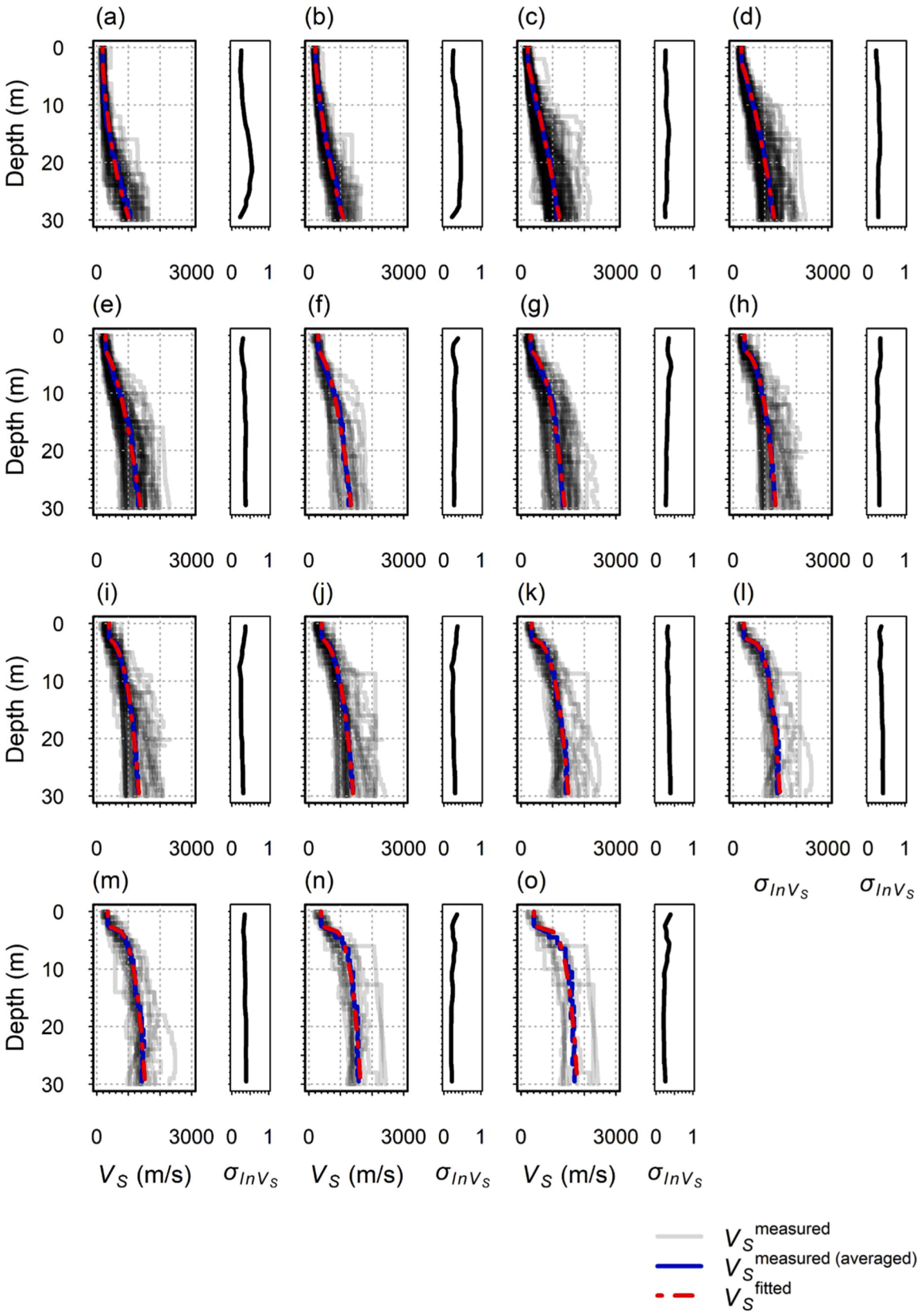

Fig. 5. Individual V_S profiles (transparent gray, solid lines) for each V_{S30} group of $Z_{760} \leq 30$ m alongside the averaged V_S profiles (blue, solid line) and the fitted V_S profiles (red, dash-dotted line). Constant, average values were computed within 0–2.5 m. The logarithmic standard deviation of individual V_S profiles ($\sigma_{\ln V_S}$) with depth is shown by black solid line on the right of each V_S profile panel.

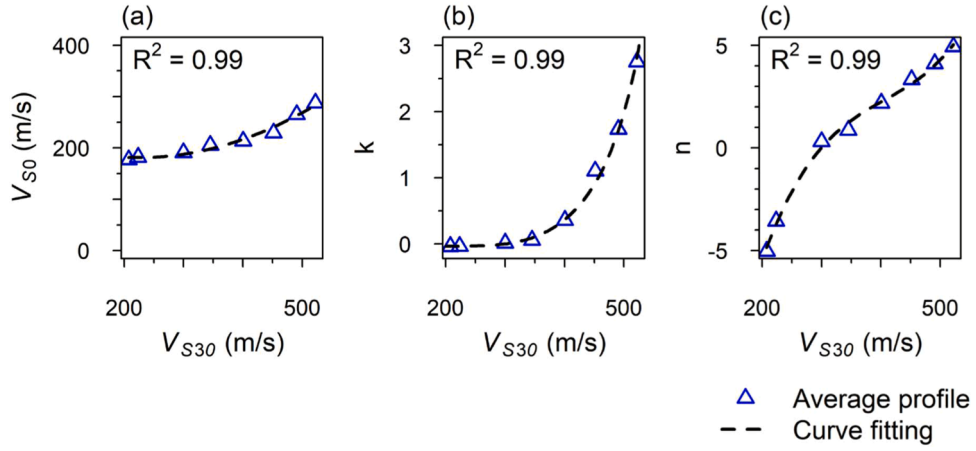

Fig. 6. Relationship between V_{S0}, k, n derived from the fitting and V_{S30} of averaged V_S profiles and their functions for $Z_{760} > 30$ m.

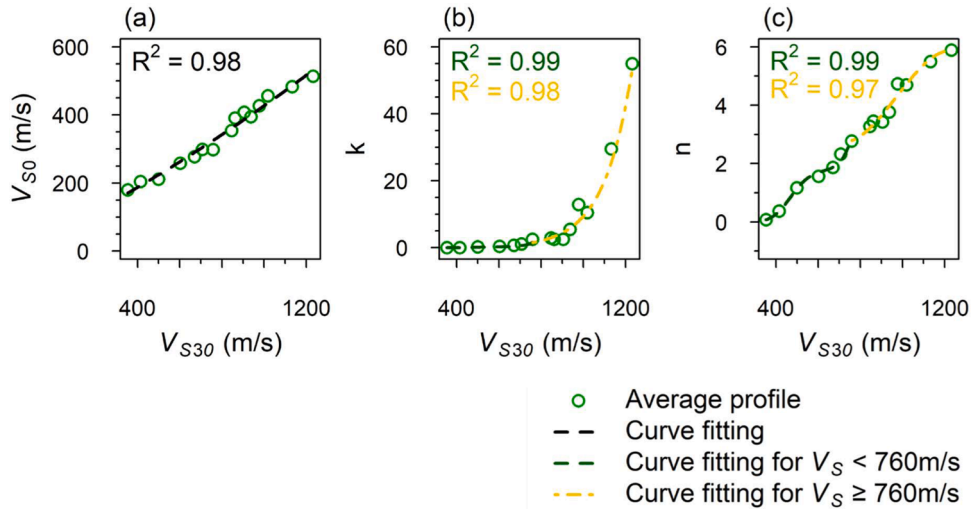

Fig. 7. Relationship between V_{S0}, k, n derived from the fitting and the V_{S30} of the averaged V_S profiles and their functions for $Z_{760} \leq 30$ m (Two functions for k and n at $V_{S30} = 760$ m/s).

Table 3
V_{S30} of the V_S profiles of test set, goodness-of-fit scores corresponding to this study ($gof_{V_S}^{This\ study}$) and Shi and Asimaki (2018) ($gof_{V_S}^{SA18}$) for $Z_{760} > 30$ m.

No.	V_{S30} (m/s)	$gof_{V_S}^{This\ study}$	$gof_{V_S}^{SA18}$
1	251.2	8.1	6.8
2	272.6	9.7	8.2
3	278.9	9.6	8.9
4	315.6	9.1	8.7
5	367.9	9.5	8.6
6	382.0	9.1	7.7
7	433.9	8.7	8.3
8	472.0	9.2	7.8
9	472.9	8.9	9.0
10	551.7	9.5	8.4

least squares method for $Z_{760} > 30$ m and $Z_{760} \leq 30$ m, as shown in Figs. 6 and 7, respectively. The functional expressions for $Z_{760} > 30$ m are as follows:

$$V_{S0} = a_1(V_{S30})^2 + a_2(V_{S30}) + a_3 \quad (3)$$

$$k = \exp\left(b_1(V_{S30})^3 + b_2(V_{S30})^2 + b_3(V_{S30}) + b_4\right) + b_5 \quad (4)$$

$$n = c_1(V_{S30})^3 + c_2(V_{S30})^2 + c_3(V_{S30}) + c_4 \quad (5)$$

Table 4
V_{S30} of the V_S profiles of test set, goodness-of-fit scores corresponding to this study ($gof_{V_S}^{This\ study}$) and Shi and Asimaki (2018) ($gof_{V_S}^{SA18}$) for $Z_{760} \leq 30$ m.

No.	V_{S30} (m/s)	$gof_{V_S}^{This\ study}$	$gof_{V_S}^{SA18}$
1	336.7	7.7	6.8
2	371.1	8.2	6.3
3	402.6	8.7	7.0
4	437.9	9.0	8.5
5	454.6	8.6	7.0
6	477.1	8.3	8.1
7	508.9	7.6	7.6
8	540.3	8.0	7.2
9	546.6	8.5	6.5
10	598.6	8.7	8.3
11	618.4	9.1	8.7
12	635.8	9.1	9.2
13	637.3	8.9	8.7
14	654.3	8.6	8.8
15	736.5	9.4	7.7
16	758.0	8.6	8.8
17	793.4	9.2	9.3
18	852.6	9.6	9.0
19	919.3	9.2	8.9
20	1,064.7	9.2	6.6

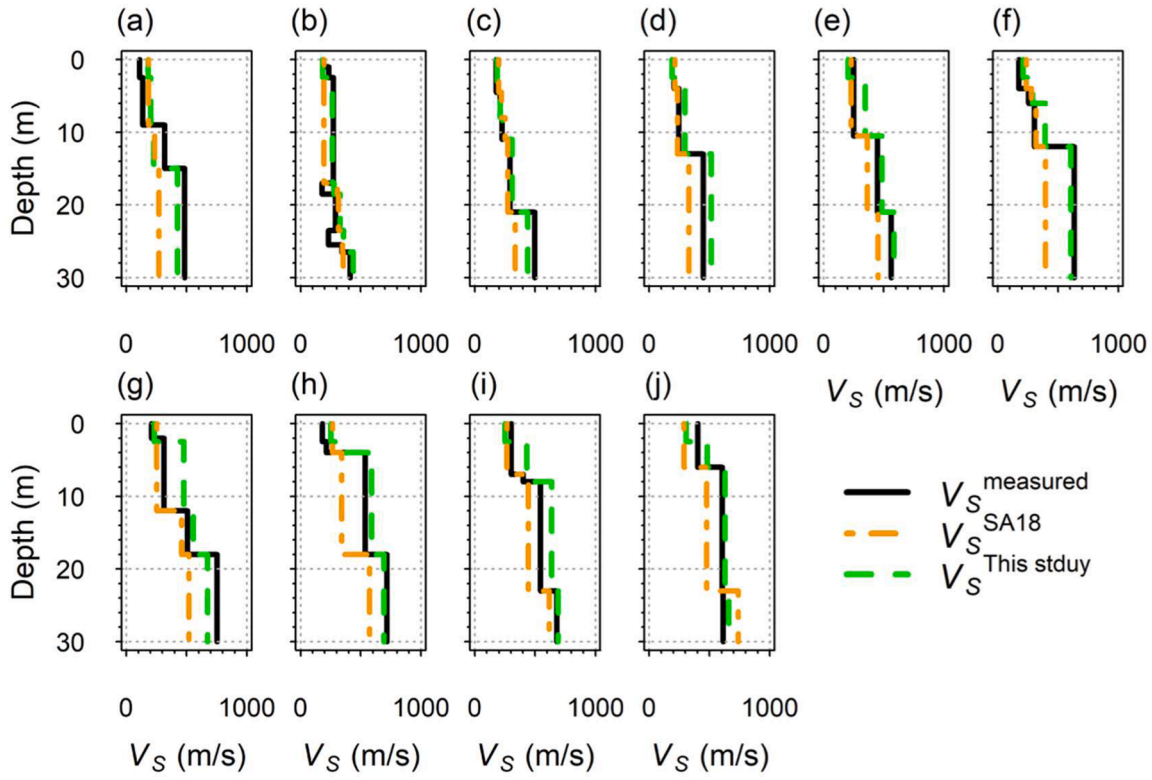

Fig. 8. Predicted V_S profiles from our model compared with the measured and predicted V_S profiles from the SA 18 model for $Z_{760} > 30$ m [The order of panel labels (a–j) correspond to the order of numbers (1–10) in Table 3].

where $a_1 = 1.142 \times 10^{-3}$, $a_2 = -5.087 \times 10^{-1}$, $a_3 = 237.74$, $b_1 = 1.576 \times 10^{-7}$, $b_2 = -2.265 \times 10^{-4}$, $b_3 = 1.238 \times 10^{-1}$, $b_4 = -24.271$, $b_5 = -3.7 \times 10^{-2}$, $c_1 = 5.122 \times 10^{-7}$, $c_2 = -6.235 \times 10^{-4}$, $c_3 = 2.692 \times 10^{-1}$, and $c_4 = -38.456$. We adopt the functional expressions for $Z_{760} \leq 30$ m as follows:

$$V_{S0} = d_1(V_{S30})^2 + d_2(V_{S30}) + d_3 \tag{6}$$

$$\begin{aligned} &k_1 = \exp\left(e_1(V_{S30})^3 + e_2(V_{S30})^2 + e_3(V_{S30}) + e_4\right) \\ &\text{for } 336.7 \text{ m/s} \leq V_{S30} \leq 758.5 \text{ m/s} \\ &k_2 = f_1 \exp(f_2(V_{S30})) \\ &\text{for } 758.5 \text{ m/s} \leq V_{S30} \leq 1,232.1 \text{ m/s} \end{aligned} \tag{7}$$

$$\begin{aligned} &n_1 = \exp\left(g_1(V_{S30})^3 + g_2(V_{S30})^2 + g_3(V_{S30}) + g_4\right) \\ &\text{for } 336.7 \text{ m/s} \leq V_{S30} \leq 758.5 \text{ m/s} \\ &n_2 = h_1(V_{S30})^3 + h_2(V_{S30})^2 + h_3(V_{S30}) + h_4 \\ &\text{for } 758.5 \text{ m/s} \leq V_{S30} \leq 1,232.1 \text{ m/s} \end{aligned} \tag{8}$$

where $d_1 = 6.013 \times 10^{-5}$, $d_2 = 3.152 \times 10^{-1}$, $d_3 = 51.593$, $e_1 = 2.581 \times 10^{-7}$, $e_2 = -4.668 \times 10^{-4}$, $e_3 = 2.863 \times 10^{-1}$, $e_4 = -60.698$, $f_1 = 5.2 \times 10^{-3}$, $f_2 = 7.5 \times 10^{-3}$, $g_1 = 1.421 \times 10^{-7}$, $g_2 = -2.659 \times 10^{-4}$, $g_3 = 1.671 \times 10^{-1}$, $g_4 = -34.699$, $h_1 = -4.811 \times 10^{-8}$, $h_2 = 1.404 \times 10^{-4}$, $h_3 = -1.272 \times 10^{-1}$, $h_4 = 39.509$. Because these parameters are highly sensitive to the V_S profiles fitted to Eq. (1), the analytical functions describing the relationship between V_{S30} and the three parameters, should exhibit minimal errors across the entire interval of V_{S30}. After searching for various nonlinear analytical functions to fit the three parameters, we selected the polynomial forms that resulted in the smallest errors. We present two functional expressions for k and n to address the different variations in k with V_{S30} prior to and subsequent to $V_{S30} = 760$ m/s, which is the boundary value that distinguishes between rock and soil sites. Notably, large k and n values are attributed to the tendency of Z_{760} to be found at shallow depths for rock sites, whereas small k and n values are accounted for by the presence of Z_{760} near 30 m depths for soil sites. The coefficient of determination (R^2) for each parameter exceeds 0.97 (indication of a good fit), as denoted in Figs. 6 and 7.

4. Evaluation of model performance and recommendations for model utilization

The V_S profiles for the test set, which were not used in curve fitting, were randomly collected from the Ministry of Interior and Safety to evaluate model performance. Here, 10 and 20 V_S profiles were considered for $Z_{760} > 30$ m and $Z_{760} \leq 30$ m, respectively. The V_{S30} values of the compiled V_S profiles are evenly distributed, as listed in Tables 3 and 4. The V_S profiles predicted using Eqs. (1) and (3)–(8) with the derived model parameters (this study) are compared with those predicted by the SA 18 model for the collected test set. Figs. 8 and 9 present the V_S profiles of the test set (black solid line, measured), this study (green dashed line), and the SA 18 model (orange dash-dotted line) for $Z_{760} > 30$ m and $Z_{760} \leq 30$ m, respectively. The predictions of V_S profiles from this study mostly show more proximity to the V_S profiles of the test set than those of the V_S profiles by the SA 18 model for both $Z_{760} > 30$ m and $Z_{760} \leq 30$ m, thereby validating the performance of our model.

To qualitatively evaluate the model performance, we measured the goodness of fit (gof_{V_S}) of the predicted V_S profile, introduced by Shi and Asimaki (2018), as follows:

$$gof_{V_S} = 10 - 10erf\left(\frac{4\left|lnV_S^{predicted} - lnV_S^{measured}\right|}{\left|lnV_S^{measured}\right|}\right) \tag{9}$$

Following the calculation of gof_{V_S} at each depth (1-m interval), we averaged them over the entire depths. A gof_{V_S} score of 10 indicates a perfect fit, whereas a score approaching 0 indicates a poor fit. The gof_{V_S} scores for this study and the SA 18 model against the test set are listed in Tables 3 and 4, respectively. The gof_{V_S} score of this study ranges as 8.1–9.7 for $Z_{760} > 30$ m, whereas that of the SA 18 model varies as 6.8–9.0. For $Z_{760} \leq 30$ m, the scores of this study and the SA 18 models are 7.7–9.6 and 6.8–9.3, respectively. This indicates that our model

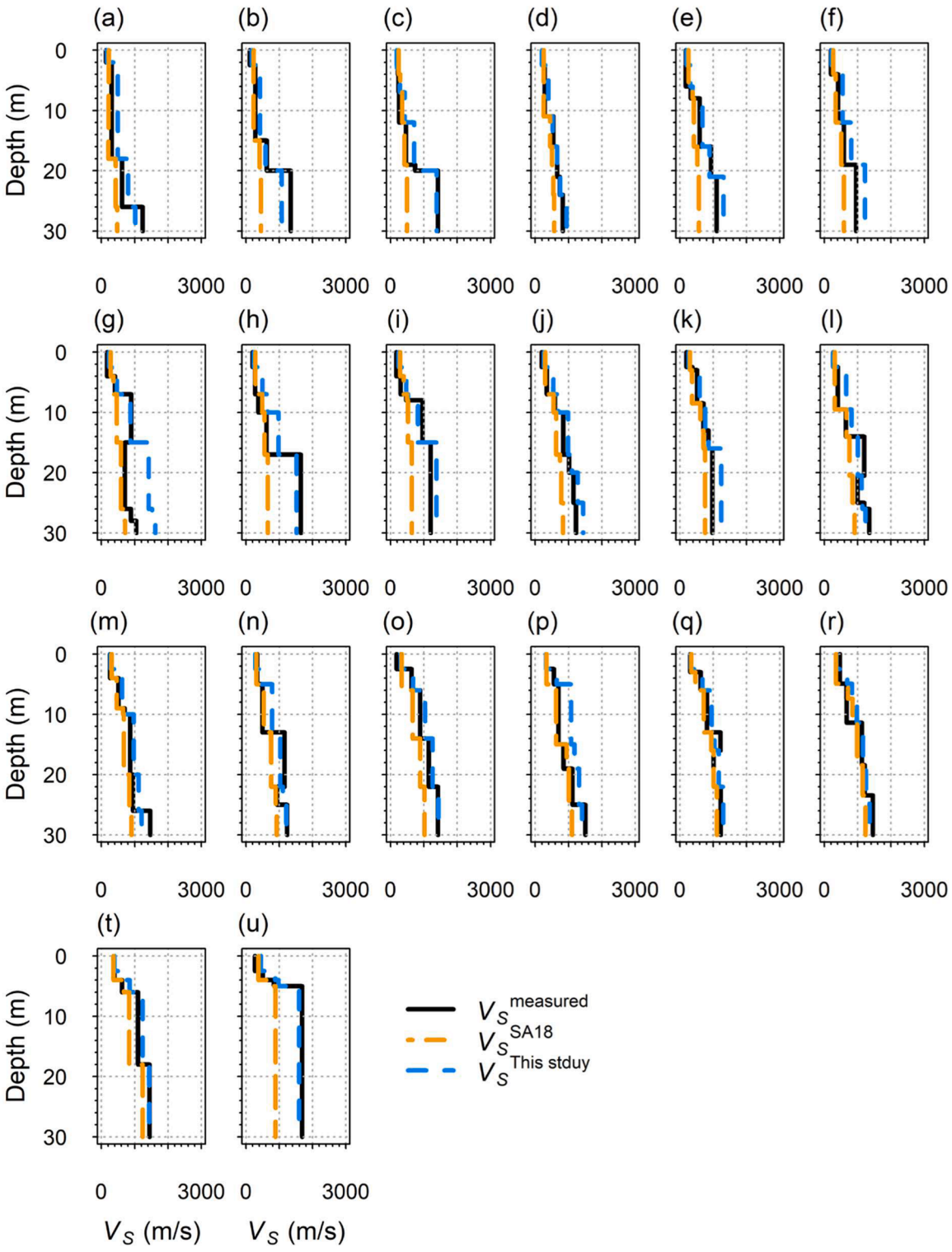

Fig. 9. Predicted V_S profiles from our model compared with the measured and predicted V_S profiles from the SA 18 model for $Z_{760} \leq 30$ m [The order of panel labels (a – t) correspond to the order of numbers (1–20) in Table 4].

significantly improved the capability of predicting V_S profiles in South Korea.

We proposed the analytical function [Eq. (1)] using the model parameters [Eqs. (3)–(8)] capable of generating synthetic V_S profiles, which are probabilistically representative of the V_S profiles in South Korea. The aim was to account for the spatial variability in site amplification for a preliminary assessment. This model assumes an increasing V_S with depth. Note the following, applicable V_{S30} ranges: $210 \leq V_{S30} \leq 520$ m/s for $Z_{760} > 30$ m and $355 \leq V_{S30} \leq 1{,}230$ m/s for $Z_{760} \leq 30$ m. However, it should be caveated against extrapolating V_S profile beyond 30 m depths, as such data were not included in the fitting process. If the extrapolation of V_S at depths below 30 m using the proposed model is required, it is recommended that the theoretical dispersion curve computed from the Thomson-Haskell (Thomson, 1950; Haskell, 1990) forward solution for the extrapolated V_S profile be compared with the experimental dispersion curve obtained from MASW and MAM at the

target site.

The proposed model is expected to be utilized alongside the following methods for V_{S30} estimation. First, it has been demonstrated that V_{S30} can be inferred from geology and geomorphology (called a proxy) (Matsuoka et al., 2006; Wald and Allen, 2007; Allen and Wald, 2009). Recently, Choi et al. (2022) proposed a proxy-based estimation method for V_{S30}, derived from proxies and V_S profiles for regions in South Korea. Second, V_{S30} can be predicted using an empirical relationship between V_{S30} and the fundamental site frequency inferred from the horizontal-to-vertical spectral ratio (HVSR) (f_{0_HVSR}) for regions in South Korea, as suggested by Ahn et al. (2021). These predicted V_{S30} values can be utilized in this model to predict the median V_S profiles at target sites in South Korea. If $V_{S30} < 760$ m/s (a soil site), it is recommended to consider both cases of $Z_{760} > 30$ m and $Z_{760} \leq 30$ m. Third, Passeri et al. (2020) compared theoretical dispersion curves for the V_S profiles randomized by Toro (1995) model with experimental dispersion curves (called site signatures) for validating their statistical model of V_S profile. The theoretical dispersion curve for a V_S profile can be obtained from the forward problem implemented in Dinver (Wathelet, 2008) of Geopsy (Wathelet et al., 2020). Hence, when experimental dispersion curves previously obtained by SASW/MASW or MAM tests are available near the target sites, the V_S profiles from this model can be better predicted by searching for the theoretical dispersion curve generated using suites of V_{S30} values that optimally fit the experimental dispersion curve (with the lowest misfit). Finally, when V_S profiles previously evaluated at a site adjacent to the target sites are accessible, this model can be employed more accurately with the given V_{S30} and Z_{760}.

5. Limitations

The predictive model of V_S profile consists of two components: 1) median V_S at depths (representing the velocity model) and 2) layer thickness at depths (i.e., the relationship between layer thickness and depth, denoting the layer thickness model). Incorporating the layer thickness model into the velocity model provides a better prediction of the V_S profile. However, this study is limited by the lack of a layer thickness model derived from a dataset of Korean sites. It is recommended to utilize the layer thickness model of Toro (1995) by obtaining the parameters of the Toro (1995) layer thickness model with the dataset of Korean sites if a higher resolution of V_S profile prediction is required. Furthermore, the extrapolation performance of our model was not evaluated (e.g., the prediction of V_S profile outside the V_{S30} range considered in this study and V_S prediction at depths greater than 30 m), and the predicted V_S profiles were not validated in terms of the amplification factor. These limitations will be addressed in future research by analyzing the V_S profile datasets in terms of layer thickness to develop layer thickness models, populating V_S profiles outside the dataset used in this study to validate the model's performance of extrapolation and estimating shear-wave transfer functions based on linear viscoelastic theory (Kramer, 1996) for soil amplification validation.

6. Conclusions

This study derived the parameters (V_{S0}, k, n) of the SA 18 model, contingent on V_{S30}, by fitting the collected 702 V_S profiles in the regions of South Korea to the model. This prediction model is essential for considering the spatial variability of V_S profiles at a site for site amplification assessments. The empirical relationships of the model parameters were separated from the Z_{760} value because the V_S profiles database was typically divided into two categories representing engineering bedrock locations within or beyond a 30 m depth. After grouping the V_S profiles based on V_{S30} values in each category, the averaged V_S profiles of V_{S30} groups were fitted to the SA 18 model, and then V_{S0}, k, and n were regressed on the V_{S30} values of the averaged V_S profiles. The V_S profiles predicted from the derived model parameters were similar to the measured V_S profiles, whereas the predictions of V_S profiles by the SA 18 model were not in good agreement with the measured V_S profiles. The averaged gof_{V_S} score for the SA 18 model was approximately 8.5 and 8.0 for $Z_{760} > 30$ m and $Z_{760} \leq 30$ m, respectively. Conversely, incorporating our model parameters resulted in the average gof_{V_S} scores of approximately 9.0 and 8.8 for $Z_{760} > 30$ m and $Z_{760} \leq 30$ m, respectively, indicating an improvement in predictive performance. Utilization of this model was expected in conjunction with a proxy-based estimation of V_{S30}, an empirical correlation between V_{S30} and f_{0_HVSR}, and experimental dispersion curves or V_S profiles available from sites near the target sites.

Declaration of competing interest

The authors declare that they have no known competing financial interests or personal relationships that could have appeared to influence the work reported in this paper.

Acknowledgment

This work was supported by KOREA HYDRO & NUCLEAR POWER CO., LTD (no. 2022-Tech-03).

References

Ahn, J.-K., Kwak, D. Y., & Kim, H.-S. (2021). Estimating V_{S30} at Korean Peninsular seismic observatory stations using HVSR of event records. *Soil Dynamics and Earthquake Engineering, 146*, Article 106650. https://doi.org/10.1016/j.soildyn.2021.106650

Allen, T. I., & Wald, D. J. (2009). On the use of high-resolution topographic data as a proxy for seismic site conditions (V_{S30}). *Bulletin of the Seismological Society of America, 99*, 935–943. https://doi.org/10.1785/0120080255

Ansal, A., Tönük, G., & Kurtuluş, A. (2018). Implications of site specific response analysis. In *Recent Advances in Earthquake Engineering in Europe: 16th European Conference on Earthquake Engineering-Thessaloniki 2018* (pp. 51–68). Springer. https://doi.org/10.1007/978-3-319-75741-4_2.

Choi, I., Yoo, B., & Kwak, D. (2022). Development of Korean Peninsula V_{S30} map based on proxy using linear regression analysis. *KSCE Journal of Civil and Environmental Engineering Research, 42*, 35–44. https://doi.org/10.5194/egusphere-egu25-1009

FEMA. (2020). *2020 NEHRP (National Earthquake Hazards Reduction Program) recommended seismic provisions: Design examples*. U.S. Department of Homeland Security. Washington, DC, USA: Building Seismic Safety Council of the National Institute of Building Sciences.

Garofalo, F., Foti, S., Hollender, F., Bard, P., Cornou, C., Cox, B., … Sicilia, D. (2016). "InterPACIFIC project: Comparison of invasive and non-invasive methods for seismic site characterization. Part II: Inter-comparison between surface-wave and borehole methods". *Soil Dynamics and Earthquake Engineering, 82*, 241–254. https://doi.org/10.1016/j.soildyn.2015.12.009

Haskell, N. A. (1990). The dispersion of surface waves on multilayered media. *Vincit Veritas: A Portrait of the Life and Work of Norman Abraham Haskell, 30*, 86–103. https://doi.org/10.1029/sp030p0086, 1905–1970.

Kim, D.-S., & Yoon, J.-K. (2006). Development of new site classification system for the regions of shallow bedrock in Korea. *Journal of Earthquake Engineering, 10*, 331–358. https://doi.org/10.1080/13632460609350600

Kramer, S. L. (1996). *Geotechnical earthquake engineering*. Pearson Education India.

Marafi, N. A., Grant, A., Maurer, B. W., Rateria, G., Eberhard, M. O., & Berman, J. W. (2021). A generic soil velocity model that accounts for near-surface conditions and deeper geologic structure. *Soil Dynamics and Earthquake Engineering, 140*, Article 106461. https://doi.org/10.1016/j.soildyn.2020.106461

Matsuoka, M., Wakamatsu, K., Fujimoto, K., & Midorikawa, S. (2006). Average shear-wave velocity mapping using Japan engineering geomorphologic classification map. *Structural Engineering/Earthquake Engineering, 23*, 57–68. https://doi.org/10.2208/jsceseee.23.57s

Passeri, F., Foti, S., & Rodriguez-Marek, A. (2020). A new geostatistical model for shear wave velocity profiles. *Soil Dynamics and Earthquake Engineering, 136*, Article 106247. https://doi.org/10.1016/j.soildyn.2020.106247

Pehlivan, M., Hashash, Y., Harmon, J., Rathje, E., Stewart, J., Silva, S., Campbell, K., & Nikolaou, S. (2015). Influence of shear wave velocity reversals on one-dimensional site response of spatially varied profiles. In *6th International Conference on Earthquake Geotechnical Engineering 1–4 November 2015*.

Rathje, E., Pehlivan, M., Gilbert, R., & Rodriguez-Marek, A. (2015). Incorporating site response into seismic hazard assessments for critical facilities: A probabilistic approach. *Perspectives on Earthquake Geotechnical Engineering: In Honour of Prof. Kenji Ishihara*, 93–111. https://doi.org/10.1007/978-3-319-10786-8_4

Rathje, E. M., Kottke, A. R., & Trent, W. L. (2010). Influence of input motion and site property variabilities on seismic site response analysis. *Journal of Geotechnical and Geoenvironmental Engineering, 136*, 607–619. https://doi.org/10.1061/(asce)gt.1943-5606.0000255

Shi, J., & Asimaki, D. (2018). A generic velocity profile for basin sediments in California conditioned on V_{S30}. *Seismological Research Letters, 89*, 1397–1409. https://doi.org/10.1785/0220170268

Thomson, W. T. (1950). Transmission of elastic waves through a stratified solid medium. *Journal of Applied Physics, 21*, 89–93. https://doi.org/10.1063/1.1699629

Toro, G. (1995). Probabilistic models of site velocity profiles for generic and site-specific ground-motion amplification studies. *Technical Rep*, Article 779574.

Vrettos, C. (1996). Simple inversion procedure for shallow seismic refraction in continuously nonhomogeneous soils. *Soil Dynamics and Earthquake Engineering, 15*, 381–386. https://doi.org/10.1016/0267-7261(96)00012-7

Wald, D. J., & Allen, T. I. (2007). Topographic slope as a proxy for seismic site conditions and amplification. *Bulletin of the Seismological Society of America, 97*, 1379–1395. https://doi.org/10.1785/0120060267

Wathelet, M. (2008). An improved neighborhood algorithm: parameter conditions and dynamic scaling. *Geophysical Research Letters*, 35. https://doi.org/10.1029/2008gl033256

Wathelet, M., Chatelain, J. L., Cornou, C., Giulio, G. D., Guillier, B., Ohrnberger, M., & Savvaidis, A. (2020). Geopsy: A user-friendly open-source tool set for ambient vibration processing. *Seismological Research Letters, 91*, 1878–1889. https://doi.org/10.1785/0220190360